Journal of Hazardous Materials 161 (2009) 1265–1280

Contents lists available at ScienceDirect

Journal of Hazardous Materials

journal homepage: www.elsevier.com/locate/jhazmat

Accidents involving liquids: A step ahead in modeling pool spreading, evaporation and burning

Sara Brambilla, Davide Manca*

Politecnico di Milano, Dipartimento di Chimica, Materiali e Ingegneria Chimica "Giulio Natta", Piazza Leonardo da Vinci 32, 20133 Milano, Italy

ARTICLE INFO

Article history:
Received 20 November 2007
Received in revised form 10 March 2008
Accepted 21 April 2008
Available online 3 May 2008

Keywords:
Industrial accidents
Simulation of liquid spreading
Pool fire
Model validation

ABSTRACT

The manuscript focuses on the modeling of industrial accidents involving liquid substances, *i.e.* liquid pools. The paper discusses how to improve Webber's model (1990) for evaluating the liquid pool dynamics in terms of spreading (onto land and water) and evaporation rates. In particular, our attention was devoted to the following points: friction term in presence of film boiling; evaluation of the friction velocity; determination of the wind profile index; evaluation of the conductive heat flux; the pool radius dynamics; turbulent mixing onto water; dispersion model input data. The paper presents, also, how to couple the proposed model to the pool burning dynamics. This allows simulating the burning of a spreading pool. Thanks to its prompt response in terms of CPU time, the proposed model is helpful not only under risk assessment or under emergency preparedness, but also during accident response. A comparison between experimental data and the model predictions validates the model effectiveness in simulating real accidental events.

1. Introduction

This paper deals with the modeling of a liquid pool, originated from an industrial accident involving a liquid phase. In particular, we discuss the modifications brought to an existent model [1] on pool spreading and evaporation. The original model from Webber was also extended with a model of pool fire. Such changes were devoted to improve the phenomenological description and to fulfill a particular constraint: the real-time simulation of accidents for risk assessment, emergency preparedness, operators training, and, in particular, emergency response. Within this context, the expression "real-time simulation" conveys the idea that the CPU time required to simulate an accident is negligible with respect to the characteristic time of the described phenomenon.

The overall model allows simulating and hence determining the dynamics of large-scale industrial and transport accidents, by providing a quantitative estimation of the accident consequences. Thanks to the real-time feature, the model is helpful whenever a prompt response is needed (*e.g.* during the emergency response).

Before discussing the main features of the manuscript, a historical overview of the state of the art of accident modeling is presented (Section 1.1). An in-depth explanation about the CPU time constraint follows (Section 1.2).

Section 2 presents a discussion about existing models and their limitations, with a particular attention to common mistakes. Some lessons learned are finally reported (Section 2.5). Since we are not proposing a completely innovative model, (we preferred to improve the Webber's one), a discussion about additions, modifications and the way for filling the gaps of the original model is reported (Section 3). Actually, the original model from Webber [1] is not presented. For any further details, the reader should refer to the original manuscript. Finally, Section 4 compares simulation output data with two sets of experimental data concerning the water spreading onto a rough surface [2] and liquefied natural gas (LNG) spreading onto water and burning [3].

1.1. Historical overview

Accidents modeling and their consequences estimation are not a new topic. Studies in this field begun some decades ago (*e.g.* [4,5]), due to the increasing amount of chemicals handled, processed and transported world wide and the growing public concern on safety and, more recently, on terrorism. Among the possible accident outcomes, the paper considers only the modeling of accidents involving spreading, evaporation and burning of liquid pools.

As reported by van der Bosch [6], earlier studies on liquid releases were focused only on particular aspects and were developed to describe isolated specific physical or chemical phenomena. From a detailed literature analysis, it is possible to observe that the attention was devoted to investigate separately: the spreading

* Corresponding author. Tel.: +39 02 23993271; fax: +39 02 70638173.
E-mail address: davide.manca@polimi.it (D. Manca).

0304-3894/$ – see front matter © 2008 Elsevier B.V. All rights reserved.
doi:10.1016/j.jhazmat.2008.04.109

Nomenclature

A	pool area (m^2)
A', A''	first and second time derivatives of pool area (m^2/s); (m^2/s^2)
c, c_1, c_2, c_3	constants (–)
c_p	specific heat (J/kg K)
C_1, C_2	constants (–)
$D_{f,film}$	friction coefficient in case of film boiling (–)
D	pool diameter (m)
D'	flame drag diameter (m)
Da	Damkholer number (–)
$D_{c,f}$	conductive heat flux in case of film boiling (W/m^2)
E	surface emissive power (W/m^2)
E_C	surface emissive power of the clear flame zone (W/m^2)
E_{Soot}	soot surface emissive power (W/m^2)
Fr	Froude number (–)
F_S	fraction of the generated heat radiated from the flame surface (–)
F_T	turbulence factor (–)
g	gravity (m/s^2)
g'	reduced gravity (m/s^2)
G	green function (–)
h	pool mean height (m)
h_{act}	actual heat transfer coefficient between water and the pool (W/m^2 K)
h_{min}	pool minimum height (m)
h_q	heat transfer coefficient between water and the pool in quiescent conditions (W/m^2 K)
k_{mass}	mass transfer coefficient (m/s)
$k\beta$	attenuation coefficient (–)
L_C	clear flame length (m)
L_F	flame length (m)
L_O	obscured flame length (m)
$\dot{m}$	mass flux (kg/m^2 s)
MW	molecular weight (kg/kmol)
n	wind profile index (–)
P_v	vapor pressure (Pa)
q	heat flux (kW/m^2)
Q_c	conductive heat flux (kW)
r	pool radius (m)
r_{st}	stoichiometric mass ratio (–)
R	ideal gas constant (J/mol K)
Re	Reynolds number (–)
Sc	Schmidt number (–)
t	time (s)
T	temperature (K)
u	radial pool velocity (m/s)
u_F^*	dimensionless burning rate (–)
u_P^*	friction velocity above the pool (m/s)
u_w	wind speed at ten meters height (m/s)
V	pool volume (m^3)
x	ratio between the clear and total flame length (–)
$\vec{x}$	vector identifying the generic pool area (m^2)
y	vapor molar fraction (–)
z	vertical coordinate above the surface (m)
z_d	surface depth beneath the pool (m)
$z_{0,P}$	pool surface roughness (m)

Greek letters

Δ	relative density (–)
ΔH_c	heat of combustion (J/kg)
ΔH_{ev}	latent heat of vaporization (J/kg)
$\Phi(t)$	temperature difference (K)
α	thermal diffusivity (m^2/s)
α_e	air entrainment (–)
χ_{Sc}	function of Schmidt number (–)
δ_c	concentration boundary layer thickness (m)
δ_{film}	vapor film thickness in case of film boiling (m)
ε	parameter (–)
ϕ_2	friction term (–)
η	mass fraction of entrained air reacting with the fuel (–)
κ	von Karman constant (–)
λ	thermal conductivity (W/m K)
μ	dynamic viscosity (kg/m s)
ν	kinematic viscosity (m^2/s)
θ	flame tilt angle (–)
ρ	density (kg/m^3)
τ	shear stress (N/m^2)

Subscripts

10	referred to the wind speed measured at ten meters height
∞	asymptotic value
a	air
c	combustion
ev	evaporative
L	liquid phase
s	surface beneath the pool
T	turbulent
V	vapor phase
w	water

of liquids onto water [5,7,8], onto either smooth surfaces [9] or rough surfaces [10]; the evaporation of pools [11,12]; the burning of pools [13–16]. On the other hand, some models describe only a class of substances, for example liquefied natural gas [3,15,17] or oil [5,7]. In such studies, the researchers isolated a particular feature of the whole phenomenon and developed *ad-hoc* models that are not interconnected to describe the complete phenomenology. The approach of those authors allows overcoming the intrinsic difficulties in the modeling activity, that are due to the fact that the involved phenomena develop on different time scales, making the problem stiff and posing some numerical troubles to the solution. By separating the phenomena, this multi-scale problem is not present, but the effectiveness in representing realistic accidents is greatly reduced.

On the contrary, the model proposed in this manuscript describes the whole phenomenology of pool spreading, evaporation and burning, by interconnecting and tackling the different phenomena. We also made some improvements to the Webber's model, in accordance with the recent innovations in this field. Our efforts were devoted to blend the best features of previous models into a unified model, capable of dealing with a wide range of conditions and substances. We chose Webber's model even if other models are present in the literature (*e.g.* [18,19]) because it has the soundest theoretical basis. For the time being, the proposed model does not account for mixtures.

1.2. Dynamic accident simulation

As aforementioned, a specific feature drove the development of the model: the simulation time had to be negligible, meaning

that the CPU time taken to perform an accident simulation of 1-h should be reduced to some seconds. Such a feature was motivated by the purpose to couple an "accident simulator" (*i.e.* the program framework that is described in this paper) to a dynamic simulator of chemical processes. This complex interaction allows improving the effectiveness of operators training, accident investigation and safety management. By doing so, possible interactions (feedbacks) between the accident and the process can be better assessed. For example, the proposed interaction allows describing the fact that if a flammable liquid is emitted by an accidental hole in a pipe, it forms a spreading pool that starts burning. The heat radiated by the flame to the surrounding equipment may increase both temperature and pressure, hence affecting the liquid emission rate. This biunique interaction can significantly enhance the process understanding and control, as well as the emergency preparedness and response in industrial sites.

As far as the operators training is concerned, a trainer can adopt this tool to supervise the activities of trainees, while judging the operator's knowledge of procedures and his/her response to unusual situations without affecting the real process or damaging any process units. With reference to accident investigation, the aforementioned coupling allows examining the evolution of process variables, when an accident occurs, as well as reconstructing the accident dynamics to forecast and mitigate the effects of future accidents and/or prevent them. This tool is also useful, under emergency preparedness, to better plan the emergency response.

2. Remarks on existing models

As mentioned above, several models on industrial accident simulation are reported in the literature, but also some mistakes and misconceptions were introduced and propagated through the years. This section discusses some examples of frequent mistakes made either when modeling or when adopting a model to simulate a specific phenomenon.

According to Webber [20,21], a number of authors misunderstood the work of Fay on the spreading regimes of an oil slick onto water [5]. In addition, some of them confused the phenomenology onto water and land and they applied the model to substances and surfaces not investigated by Fay, without any justifications and experimental verifications. These topics are discussed in Sections 2.1 and 2.2. The use of explicit correlations and the range of models validity are also analyzed in Sections 2.3 and 2.4 respectively. Finally, Section 2.5 reports some lessons learned.

2.1. Gravity-inertial vs. gravity-front resistance regime

With reference to oil spreading onto water, Webber [21] argued that the idea that an equation in the form:

$$\frac{dr}{dt} \sim \sqrt{g'h} \tag{1}$$

somehow corresponds to a pure gravity-inertial regime is "*one of the most widely propagated pieces of nonsense*". Conversely, this equation represents the gravity-front resistance, while the balance between gravity and inertia is described by the equation:

$$\frac{d^2r}{dt^2} = \frac{2g'h}{r} \tag{2}$$

Several authors adopted Eq. (1) to model the spreading onto water while asserting that they considered the gravity-inertial regime (*e.g.* [8,19,22]). This is not just a formal point: the integration of Eqs. (1) and (2) leads to completely different results. In the former case:

$$\frac{dr}{dt} \sim \sqrt{g'h} \Rightarrow r \sim \sqrt{t}$$

while in the latter:

$$\frac{d^2r}{dt^2} = \frac{2g'h}{r} \Rightarrow r \sim t$$

Consequently, it is conceptually wrong to assert that one is solving the gravity-inertia balance equation if the proposed solution is $r \sim \sqrt{t}$.

The faulty conjecture in the work of Fay [5], which leads to the wrong mathematical conclusion starting from Eq. (2), is that $d^2r/dt^2 \sim r/t^2$. By integrating rigorously Eq. (2) instead of simplifying it, and by introducing the proper integration constant, the $r \sim t$ dependence may be found, even if it is wrong from a phenomenological point of view [21].

In addition, Webber and Brighton [9] derived the same erroneous dependency, but they stated that this is not how real pools behave, as they neglected resistance. Nonetheless, they added that it is the right answer under the hypothesis of energy conservation for the gravity-inertial regime.

It should be underlined that the $r \sim \sqrt{t}$ dependency is extremely well observed in experimental tests. Consequently, the dependence of radius from the square root of time is not under discussion. It is important to remark that such a dependency did not originate from a balance between gravity and inertia (Eq. (2)). Such a proportionality represents the gravity-front resistance regime for spreading onto water and it can be obtained by solving the gravity-front resistance equation in the form of Eq. (1).

For the sake of clarity, Webber [21] argued that the $r \sim \sqrt{t}$ behavior is neither valid in the early stages, where acceleration (*i.e.* inertial regime) is important, nor in the later stages, where the pool becomes so thin that shear effects over the whole area of the pool start dominating the resistance (viscous regime). Actually, we do not want to diminish the work of Fay and other authors, but we want to clarify a few theoretical issues. Some assumptions that were necessary in the past to find the analytical solution of a differential equations system (*e.g.* in 1969, when Fay published his work) are neither justified today nor are required, thanks to the computing power of common desktop computers and modern numerical routines. Consequently, we tried to drive the reader towards the models that are as general as possible.

2.2. Spreading onto land

For spreading onto water, Eq. (1) is probably much better than the gravity-inertia equation (Eq. (2)), just because it models the front resistance onto water.

The problem with confusing the regimes comes when spreading onto land comes in hand. If it is accepted that Eq. (1) is a front resisted model, then there is not the temptation to use it for spreading onto land, where there is no displaced water and air has a negligible viscosity to produce any significant resistances. However, if one thinks that Eq. (1) is a gravity-inertial model, then he/she is immediately tempted to use it as a spreading model onto land.

An example of this misconception is the model adopted by DNV and implemented in the commercial software PHAST [19]. For gravity spreading onto land, PHAST adopts the following equation:

$$\frac{dr}{dt} = \sqrt{2g(h - h_{\min})} \tag{3}$$

This equation cannot accurately model flows resisted by ground friction and consequently it will predict spreads that are initially too slow and that become too fast when evolving. Furthermore,

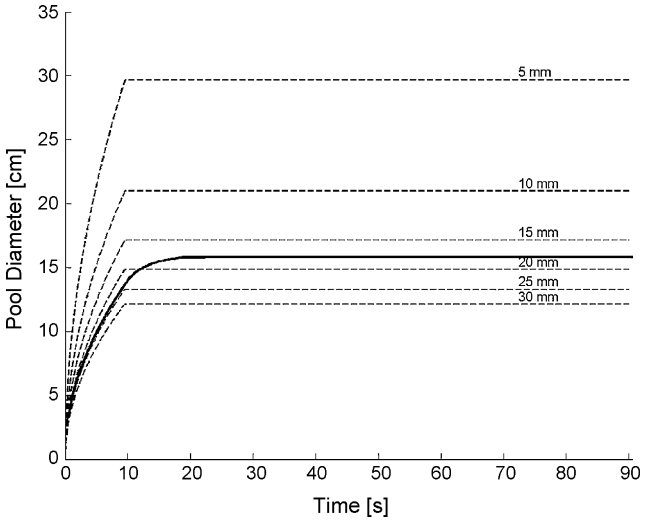

Fig. 1. Pool diameter as a function of spreading time. Webber's model (solid line); Witlox model for different values of h_{min} (dashed lines).

Eq. (3) does not describe the shrinking phenomenon. Actually, when an evaporating pool reaches the minimum height ($h = h_{min}$), it shrinks according to the principle of mass conservation, while Eq. (3) predicts a constant radius ($dr/dt = 0$).

In addition, the predictive ability of Eq. (3) is strongly related to the method selected to evaluate h_{min}. An incorrect choice produces completely misleading results. Unfortunately, the approach for evaluating h_{min} is not trivial. Witlox [19] reported a table where the value of h_{min} can be inferred from the surface typology onto which the spreading occurs. Witlox recognized that a more accurate approach must be adopted. In our opinion this represents a crucial point, since the reported values of h_{min} are not function of the physicochemical and morphological properties of the surface and only a limited number of surfaces are included (five surfaces).

To clarify this point we compared the results of Webber's model and a model in the form of Eq. (3), for different values of h_{min}. In particular, we considered a water spill onto a smooth surface (*e.g.* formica). Figs. 1 and 2 show the differences between these models: the results obtained from the integration of Eq. (3) can be completely wrong if an incorrect value of h_{min} is adopted. For example,

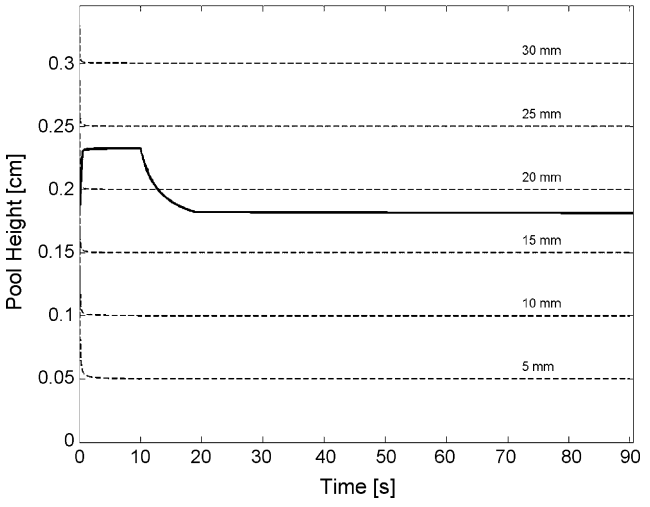

Fig. 2. Pool height as a function of spreading time. Webber's model (solid line); Witlox model for different values of h_{min} (dashed lines).

if h_{min} = 5 mm the asymptotic diameter derived from the integration of Eq. (3) is twice the experimental value (30 cm vs. 15 cm).

Webber [21] declares that a model based on Eq. (3) is wrong, although it produces the right qualitative (not quantitative) results and it is quite difficult to see how wrong the model is under the conventional operating conditions.

In conclusion, it is possible to state that:

- the gravity-front resistance model (Eq. (1)) was not developed for describing the spreading onto land. To model such a phenomenon, the friction between the substance and the underlying surface should be included in the model. The model adopted in this manuscript [1] includes this feature;
- Eq. (3) requires a method for evaluating h_{min}; otherwise, the obtained results are completely misleading (see Figs. 1 and 2).

2.3. Use of explicit equations

Independently of the correctness of a functional form expressing the radius-time dependence, Webber [21] says that using an explicit algebraic correlation for calculating that dependence prejudges the consistent solution of the other differential equations of the dynamic model, that describe the pool edge radial velocity, the pool volume and temperature time dependence.

In fact, Hoult [7] and Fannelop [18] reported explicit algebraic correlations for the radius-time dependence of oil spreading onto water. Actually, oil can be considered as a non-evaporating substance, hence the differential equations for the energy and mass balance are not needed, and the only equation describing the pool dynamics is that of spreading. In this case, the explicit, integrated form of the differential equation would not compromise the correct integration of the system of differential equations, since the differential system is not present at all.

Witlox [19] reported some functional forms similar to those from Hoult and Fannelop for modeling both non-evaporating and evaporating substances, without any restrictions. For non-evaporating pools, such correlations include the initial mass of the pool, which is constant during the spreading. In case of evaporating substances, Witlox [19] substituted the initial mass with the time-varying mass. As stated by Witlox, such formulae are based on experiments for non-volatile liquids, therefore the expressions may not be appropriate for volatile liquids. This means that the model validation with experimental data related to volatile liquids is highly recommended, but at our knowledge, it has not been performed till now.

The model proposed in this manuscript does not couple differential and algebraic equations, but it is based on a system of six differential equations. By doing so, the solution of the differential system, describing the whole phenomenon, is not compromised [21].

2.4. Validity range of models

In all the scientific fields involving a modeling activity, applying a model for the description of a specific phenomenon outside of its validity range may lead to completely misleading and erroneous results and, consequently, it is highly recommended to avoid this practice. Unfortunately, not all the literature models comply with this recommendation. As reported by Fay [15], a number of models available in the literature are based on laboratory experiments about spreading of oil pools, such as those from Hoult [7] and Fay [5], but they were erroneously extended to model LNG spreading. The suitability of the models of Hoult and Fay for LNG spills is doubtful since there are substantial differences in the physical behavior of crude oil and LNG. Moreover, the conditions that lead to the

discharge of these substances from a laboratory unit or from a marine tanker are quite different.

Accordingly to Fay [15], the main parameter that makes oil and LNG behave differently is the relative density, defined as $\Delta = (\rho_w - \rho_L)/\rho_w$. Hoult's model [7] was designed to characterize the behavior of liquids with relative density around 0.1, such as crude oils. Conversely, relative density of LNG is about 0.58, but, while oil forms non-evaporating pools, LNG pools on water will boil vigorously. Consequently, the average density of LNG pools is even more reduced with effective Δ values up to 0.8. Therefore, the behavior differences between oil and LNG are even more significant. This implies that the flow features at the pool edge are quite different for LNG compared with oil. Such a characteristic is important because it identifies the similarity parameters for non-evaporating pools [9], *i.e.* pools with the same value of the similarity parameter behave in the same manner.

Another point that makes doubtful the application of models derived from laboratory tests lies in the difference between the initial conditions of Hoult's experiments and the real pouring conditions. Laboratory tests, such as those of Fay [5] or Hoult [7], comprised an initial amount of oil contained into a bund. The pool would spread after the bund removal, *i.e.* the release was instantaneous. More likely, real accidents behave as continuous and time-dependent releases.

This means that a model derived from experimental tests (both laboratory and field tests) cannot be extended straightforward to other not yet investigated substances.

On the other hand, models developed from a phenomenological description of events must be validated against experimental data.

2.5. Lessons learned

Some mistakes and misunderstandings are reported in the scientific literature on pool spreading and evaporation, due to erroneous assumptions (hypotheses onto which the model is based) and use of models (use of a model outside its validity range domain). Even commercial and well-accepted simulation programs propagate some mistakes. For example, in PHAST [19]:

- it is erroneously stated that the spreading equation represents the gravity-inertial regime;
- the same correlation (Eq. (3)) is used to model the spreading onto land and water;
- explicit correlations expressing the radius-time dependence according to Fay's theory [5] are adopted, even if it is not recommended;
- in the formula for pool spreading, the initial pool mass was substituted with the time-varying mass, but this substitution has never been validated against experimental data for evaporating puddles;
- the spreading onto land is characterized by only the first of the three regimes identified by Fay [5], without any justifications.

From the analysis above, it is possible to state that the application of models for non-evaporating pools to evaporating ones is not straightforward. Moreover, it seems quite obvious that literature models should be applied only within their range of validity, both in terms of substances and physical conditions.

In the following sections, the conditions and hypotheses for the validity of the selected model from Webber [1] are reported and discussed in detail. In particular, we will discuss some modifications that, in our opinion, can significantly improve the modeling of the real phenomenon. These modifications are neither native of Webber's model, nor they were ever suggested by Webber. We draw our proposal on publications that are more recent.

3. The need for a unified model

With reference of pool formation and evaporation/burning, the topics discussed in the previous sections make evident that the best model consists of a system of differential equations, describing the pool dynamics in terms of geometry, mass and energy, avoiding any explicit correlations (algebraic equations). A consistent and unified model is advisable, because it allows simulating a complete accidental scenario, without the use of distinct models to describe different phenomena. The key point is that the model proposed in this manuscript has all these features.

The proposed model is based on previous, specific works, each one requiring a different set of input data. The blending and harmonization of these independent models, developed by different authors, was not trivial. However, a unified model avoids arranging the output data of a specific model to be the input data of the following one, *i.e.* we do not need to arrange the output data from a pool spreading model to be the input data for an evaporation model and eventually for a pool fire model. Actually, this is not a trivial and common feature. For example, working with PHAST, one has to provide the pool diameter to simulate a pool fire scenario.

Some efforts were also devoted to identify models capable of describing all the classes of substances while including the features related to pool spreading, evaporation and fire. For instance, Webber [1] combined spreading and evaporation, while Engelhard [23] combined pool spreading and fire.

The efforts spent by the Authors in developing a model capable of describing a wide range of conditions and substances, were aimed at avoiding any incorrect applications of the model itself. This manuscript gives an overview of the Webber's model [1], the forerunner for the proposed model, and explains the modifications introduced to improve it. Correlations to model pool fire are also presented.

In the following section, the limitations and hypotheses onto which the unified model is based are discussed. Finally, a validation between the model outcomes and experimental data is proposed.

3.1. Webber's model: overall considerations

In this section, we will not report any details of the Webber's model [1]. Instead, the hypotheses and assumptions of such a model will be discussed and justified because they are not reported explicitly in the original manuscript of Webber.

Webber's model describes the spreading and vaporization rates of a circular axisymmetric liquid pool poured either onto land or onto water. Both confined and unconfined releases are modeled, the former being more relevant for accidents in chemical plants, where columns and vessels are often surrounded by dikes to limit the extension of possible spillages.

The surface onto which the liquid spreads is assumed horizontal, flat and statistically uniform. Surfaces with varying roughness and slope are not modeled. The pool and the underlying surface are also in perfect contact.

Liquids spilled onto water are assumed to float on the surface and not to mix with or to solve into water.

The action of waves and currents is not accounted for. The only work on this topic is that of Quest Consultants and reported by ABSG Consulting Inc. [17], but it is not recommended because waves were modeled as stationary objects. Brighton [12] regarded the roughness length on water as a universal constant that describes the existence of waves. Brighton did not model the waves directly, but

he assumed that the roughness length could somehow account for them [21].

The basic structure of Webber's model is a system of six ordinary differential equations (ODE) that describe the bulk properties of a liquid pool:

- the mass conservation, in terms of pool volume, volume discharged into the pool and vaporized volume;
- the spreading, in terms of pool radius and radial velocity;
- the internal energy, in terms of pool temperature.

Within this context, the radial velocity is defined as the velocity of the pool edge. Usually, this term is derived from a hydrostatic force balance, resulting in $u \sim \sqrt{g\Delta h}$. This dependence derives from experiments where the liquid is initially confined in a bund and, after its release, the potential energy of the substance, in terms of liquid head, is turned into kinetic energy. In practical cases, Fay [15] states that the release conditions (outflow velocity, hole diameter and geometry) should dominate the radial spreading rate and an accidental spillage from a tanker would produce a pool characterized by a radial velocity which is much higher than $\sqrt{g\Delta h}$. It is possible to conclude that, often, in practical cases the radial velocity is determined by the release conditions. To evaluate the radial velocity, we considered the contribution of both pool height and release conditions, because they are usually comparable in magnitude. According to Webber's model [1], the radial velocity accounts also for the friction between the pool and the underlying surface. This feature is required to describe the real dynamics of a pool. The friction term differs for releases onto land and water, since it accounts for the different properties of these surfaces. This is quite a relevant point, since the inclusion of friction in the model reduces the extension of the pool and, consequently, the area covered by the spillage.

Webber's model [1] describes two different source typologies: the instantaneous source and the continuous, time-varying source. In case of liquid release, the time-varying source type is the most probable. The source is assumed a point source, since the emission hole is usually small with respect to the pool dimensions. In fact, for viscous fluids, such as oil, the average pool height, once the release has stopped, approaches 1 cm or less [7]. Consequently, the pool diameter is quite large (up to some hundreds of meters), even when the released mass is not so high. For instance, under the hypothesis of a 1 cm pool depth, an oil release of 10 m^3 (8 tons approximately) will reach a diameter of about 36 m.

A number of papers in the scientific literature are based on the three regimes proposed by Fay [5] for the spreading of pools. On the contrary, Webber's model does not make any differences among the three spreading regimes, and the scientific community recognizes as well that it has a better theoretical basis [17].

The spreading description by Webber is based on the shallow water equations for non-evaporating fluids [9]. In that work a self-similarity variable, describing the radial profile of pool height, is proposed, but its extension to evaporating pools is not justified. Such a variable influences the pool spreading since it is involved in the evaluation of the radial velocity. Actually, the application of this model to evaporating liquids is possible since in real cases, the radial velocity of the pool is determined by the source term, as discussed above, and hence it must not be self-similar [15,24]. This means that, even if the self-similar variable was introduced to describe non-evaporating pools, it can be used even for evaporating ones although it loses the original meaning.

Another key issue is the choice of the evaporation model. Several models are based on the correlations proposed by MacKay and Mastugu [11]:

$$\dot{m}_{ev} = \frac{k_{mass} \times P_v(T) \times MW}{RT} \tag{4}$$

where the mass transfer coefficient k_{mass} is determined experimentally. This coefficient depends on the pool diameter, the wind speed, the Schmidt and Reynolds numbers and an experimental dimensional constant [4,25–27]. The correlations by Sutton, Raj and Kawamura reported by Engelhard [23] to evaluate the evaporative flux share the same Schmidt number. According to Brighton [12], the exponent of the Schmidt number is still under discussion and there is not any sound basis for up-scaling the results, which are derived from laboratory experiments. Moreover, the use of a dimensional constant is not recommended, due to possible misinterpretations when changing the units of measure.

On the contrary, Webber's model is based on the work of Brighton [12] for modeling the evaporation from a liquid surface into the atmospheric turbulent boundary layer. The functional form is similar to the previous one and is based on the chemical and physical properties of the involved substances, the meteorological variables and the characteristics of the surface onto which the pool lies. In this case, there are not any dimensional or non-dimensional constants and, hence, Brighton's formula [12] does not depend directly from any experimental tests. The evaporation rate is expressed as:

$$\dot{m}_{ev} = \left(\frac{-MW \times P_v(T)}{RT}\right)(u_p^*)\left(\frac{\kappa}{Sc_T}\right)(1+n)G(e^{\chi_{Sc}})\left[\frac{\ln(1-y)}{y}\right] \tag{5}$$

The model was developed for pools of fixed area (confined pools). The extension to a time-dependent either expanding or contracting pool is consequently an approximation that should be acceptable as far as the pool conditions do not change significantly during the time taken by the wind to cross the pool [28].

Table 1
Proposed for improvements to Webber's model

Argument	References	Topic	Equations
Spreading	Havens, Spicer and Fay [29]	Friction term in presence of film boiling (Section 3.2.1)	(8)
Evaporation	Sutton [4], Engelhard [23]	Friction velocity (Section 3.2.2)	–
Evaporation	Lees [32]	Wind profile index Section 3.2.3)	–
Conductive heat flux	Webber [33]	Evaluation of the conductive heat flux	
Spreading and evaporation	ABSG Consulting Inc. [17]	Pool radius dynamics at the pool minimum height (Section 3.2.5)	(17)
Evaporation	Hissong [35]	Turbulent mixing onto water (Section 3.2.6)	(18)
Input data for a subsequent dispersion model	Kunsch [37]	Dispersion model input data for buoyant and neutral gases (Section 3.2.7)	(19), (21)

3.2. Improvements to Webber's model

With reference to Webber's model [1], the modifications introduced in this manuscript to the original model improve it conceptually and make it faster so as to reach an almost real-time simulation. In particular, we focused our attention on the following conceptual features:

- friction term in presence of film boiling;
- evaluation of the friction velocity;
- determination of the wind profile index;
- evaluation of the conductive heat flux;
- pool radius dynamics;
- turbulent mixing onto water;
- dispersion model input data.

These points will be discussed in detail and separately in the following sections. For a short summary of modifications and the related topics and references, see Table 1.

3.2.1. Friction term in presence of film boiling

With respect to Webber's model [1], we modified the friction term in case of film boiling. Commenting the ABSG Consulting Inc. report [17], Havens, Spicer and Fay [29], maintain that the friction of spreading LNG over water was overestimated in some cases, causing a delay in the spreading of the pool. They pointed out that Webber's approach does not account for that film boiling can occur for cryogens, especially LNG. Under the film-boiling regime, a thin layer of vapor develops between water surface and liquid pool. This vapor has a viscosity that is two orders of magnitude lower than the viscosity of the discharged liquid and three orders of magnitude lower than the viscosity of water. According to Webber, the friction coefficient is constant and this is usually correct in most circumstances. However, Webber maintains that the friction term may depend on the nature of the surface under the pool and whether or not film boiling is taking place [1]. Therefore, since the vapor film significantly reduces the friction between the liquid surfaces, we modified Webber's model accordingly. As suggested by Havens, Spicer and Fay [29], a straightforward approach is assuming complete slip between the pool and the water surface when estimating the friction from the shear stress in the vapor film. The assumption of complete slip means that the water surface remains stationary and that the velocity profile is uniform throughout the pool thickness. This approximation is justified by the fact that the vapor viscosity is much lower than the liquid viscosity. Under these hypotheses, the thickness of vapor film can be approximated by:

$$\delta_{\text{film}} = \frac{\lambda_{\text{V}}(T_{\text{w}} - T_{\text{L}})}{H_{\text{c,f}}} \tag{6}$$

where λ_{V} is the thermal conductivity of the vapor film, T_{w} and T_{L} are respectively the temperatures of water and pool, and $H_{\text{c,f}}$ is the heat flux exchanged in the film-boiling regime. The shear stress (τ) in the film is:

$$\tau = \frac{\mu_{\text{V}} u}{\delta_{\text{film}}} \tag{7}$$

The shear stress represents the friction force on the pool, per unit area of pool surface, and allows deriving the friction coefficient:

$$C_{\text{f,film}} = \frac{\tau}{\rho_{\text{L}} h} \tag{8}$$

Eventually, the friction coefficient can be introduced in the Webber's model when film boiling occurs. By doing so, friction is better modeled than in the original manuscript [1].

3.2.2. Evaluation of the friction velocity

Webber's model requires the evaluation of the friction velocities, exerted by the wind that passes over the pool and the surface onto which the pool spreads, to determine the evaporative flux and the heat exchanged by convection between the pool and the atmosphere. Rigorously speaking, the evaluation of friction velocity involves the solution of a system of three non-linear equations in the friction velocity, the Monin-Obukhov length, and the friction temperature [30]. These variables depend on a large number of parameters that may change along with the accident evolution (*e.g.* meteorological conditions). Consequently, the non-linear system should be solved at each time step of the integration of the differential system, making the numerical procedure quite time-consuming. To avoid unnecessary, time-consuming routines, the authors applied Sutton's simplified approach. According to Sutton [4], the friction velocity spans the range 3–12% of the wind velocity (measured at ten meters over the ground) depending on the surface roughness. The lower value is associated to the smoothest surfaces and the higher one to the roughest surfaces. For the surfaces of practical interest, Sutton suggests considering them as rough, but we prefer considering a surface rough if its roughness is higher than 0.02 m. van der Bosch [27] proposes a similar classification. Onto water, Sutton considers that, if the wind velocity is lower than 6–7 m/s, the water surface is practically smooth. Conversely, if the water surface is choppy, a method for calculating the height of waves should be provided. The same approach can be applied when the friction velocity over a pool must be evaluated, by considering the pool in the same way of a water expanse. Consequently, if the wind velocity is lower than 6–7 m/s the pool surface is considered practically smooth, otherwise it is regarded as rough.

We chose to infer the ratio of friction velocity and wind speed of Sutton's approach from the rigorous approach. Details are reported in the following. In addition, we considered different ratios in case of smooth and rough surfaces. By adopting these simple and explicit correlations between friction velocity and wind speed, the evaluation of Monin-Obukhov length and friction temperature is avoided during the pool dynamics computation and the solution of the non-linear system is not required. By doing so, we achieved a significant speed-up of the simulation procedure.

By means of the rigorous approach, we evaluate the variation of the friction velocity as a function of three parameters: wind speed at a reference height (10 m), surface roughness and cloud cover.

Table 2
Validation of the van Ulden and Holstlag [30] model with Coyote series data [31]

Coyote series	Friction velocity (m/s)		Friction temperature (K)		Monin-Obukhov length (m)	
	Measured	Evaluated	Measured	Evaluated	Measured	Evaluated
3	0.280	0.310	−1.02	−0.54	−6.35	−14.06
4a	0.280	0.298	−0.43	−0.44	−24.2	−15.46
4b	0.269	0.285	−0.32	−0.24	−33.3	−26.2
4c	0.328	0.380	−0.24	−0.18	−79.4	−63.4
5	0.439	0.459	−0.95	0.00	−16.5	Inf

Table 3
Input data for the comparison between the Sutton's and rigorous approaches

Data	Day-time	Night-time
Longitude	0°	0°
Latitude (north)	45°	45°
Time	2 p.m.	2 a.m.
Date	15 June	15 June
Air temperature	30 °C	18 °C
Surface temperature	40 °C	18 °C
Albedo	0.3	0.3
Soil moisture	0%	0%

The air and surface temperature, relative humidity, time and date, plant location (latitude and longitude) are also assigned and kept constant. The surface roughness was upper limited at 1 cm since the surface roughness of industrial ground is approximately 0.5 cm [27]. Two comparisons were carried out, either for day- or night-time conditions onto land.

The model for evaluating the friction velocity, the Monin-Obukhov length and the friction temperature was previously compared with the Coyote series tests [31] in order to validate it. Results are reported in Table 2.

As can be seen, the van Ulden and Holstlag [30] model is in good agreement with measured data, especially for the friction velocity, and hence it can be applied for the following simulations.

Table 3 summarizes the input data needed to evaluate the effects of wind speed (at a reference height of 10 m), of surface roughness and of cloud cover on friction velocity.

By solving the non-linear system of the detailed model, we found that both the friction velocity and the ratio between the friction velocity and the wind speed change with the identified input data. Such a ratio has a different trend for day- and night-time conditions. For day-time conditions the ratio decreases as the wind speed increases; for night-time conditions the ratio increases as the wind speed increases. In addition, the ratio varies between 6% and 25% during day-time and between 2% and 15% during night-time. Table 4 summarizes the main results.

The authors suggest the following simplified friction velocity profile:

- during day-time: 8% of the wind speed for smooth surfaces and 14% for rough surfaces;
- during night-time: 5.5% of the wind speed for smooth surfaces and 11% for rough surfaces;

Over water, the following values are suggested: 3.5% for wind speeds lower than 7 m/s (smooth sea surface), otherwise 8.5% (rough sea surface).

3.2.3. Determination of the wind profile index

In the original paper of Webber [1], the analytical sequence for evaluating the wind profile index from meteorological data is not complete (some equations are lacking and no references to other manuscripts are reported). Consequently, we suggest a simplified approach, based on the atmospheric stability classes originally proposed by Pasquill [32].

Table 4
Results of the rigorous approach

	Day-time		Nigh-time	
	Smooth surface	Rough surface	Smooth surface	Rough surface
Mean ratio (%)	7.8	14.0	5.6	11.0

The atmospheric stability class, for a given accidental scenario, is determined according to cloud cover, date, time and wind speed measured at a height of 10 m over the surface.

3.2.4. Evaluation of the conductive heat flux

To asses the hazard associated with the spillage of toxic or flammable substances, the rate of vaporization must be quantified. For boiling liquids, the evaporation rate depends on the heat flux entering the pool, while for evaporating liquids the evaporation is determined by mass transfer.

In case of boiling liquids, the heat exchanged between the pool and the underlying surface is often the most important terms in the energy balance. With reference to spillages onto land, the conductive heat flux can be evaluated through two approaches [33]: the detailed three-dimensional heat conduction model or the vertical conduction approximation. Webber [33] discussed the different boundary conditions that can be assumed to solve both models.

To understand the solutions, that differ from the conventional formulae [34], a short phenomenological introduction is necessary. Initially, the surface is at a given temperature. Under the pool spreading, due to the temperature difference between the surface and the pool, the exchanged heat flux modifies both the temperatures. In the vertical conduction approximation, only the surface under the pool modifies its temperature, while the uncovered portion remains at the initial temperature. In this case, the equation to be solved is:

$$\frac{\partial T_s}{\partial t} = \alpha \frac{\partial^2 T_s}{\partial z_d^2} \tag{9}$$

where $T_s = T_s(t, z_d, \vec{x})$; $\vec{x}$ is a two components vector representing the generic shape of the pool area ($\vec{x} \in A(t)$); and z_d is the vertical coordinate, positive in the downward direction.

In the three-dimensional model, horizontal conduction is also considered, and heat transfer between the uncovered surface and the pool occurs. The equation to be solved is:

$$\frac{\partial T_s}{\partial t} = \alpha \left[\frac{\partial^2 T_s}{\partial z_d^2} + \vec{\nabla}^2 T_s \right] \tag{10}$$

Webber [1] stated that the vertical conduction approximation is valid for $t < t_H$, where the horizontal time scale is $t_H = A/(4\pi\alpha)$. Usually, the thermal diffusivity of the surface ranges from 10^{-7} to 10^{-6} m^2/s, and, even for small pool areas, the horizontal time scale is higher than two hours. Furthermore, the three-dimensional model requires the numerical solution of two definite integrals at every call of the ordinary differential equations system. This makes the overall numerical procedure quite demanding. Moreover, Webber [33] reports that for typical grounds the horizontal conduction effect may be considered negligible, except for very small, bunded pools or relatively non-volatile liquids, or pools that have become small due to evaporation. Consequently, we chose to implement the simpler vertical conduction approximation independently from its reduced precision.

Once Eq. (9) is solved and the temperature profile is evaluated, the heat flux from the surface to the pool becomes:

$$q(t, 0, \vec{x}) = \lambda \frac{\partial T_s}{\partial z_d} \tag{11}$$

The total heat flux into the pool is:

$$Q_c(t, 0, \vec{x}) = \int_{A(t)} q(t, 0, \vec{x}) d\vec{x} \tag{12}$$

Webber [33] solved Eq. (9) assuming two distinct boundary conditions. In both cases, the pool is assumed to be at a uniform, time dependent, temperature.

The former boundary condition is based on the hypothesis of perfect thermal contact between the pool and the surface. This means that the pool and the surface layer, which is in contact with the pool, are at the same temperature. The latter boundary condition is based on the hypothesis that the heat flux into the pool is proportional to the temperature difference between the pool and the ground. In this case, an estimation of the heat transfer coefficient has to be provided. As suggested by Webber [33], the solution derived by the first boundary condition provides an adequate estimate of the conductive heat flux if the vaporization time lasts more than approximately 100 s. Consequently, we chose the vertical conduction approximation, applying the boundary condition related to perfect thermal contact.

The solution proposed by Webber [33] differs from the common solution found in the literature (*e.g.* [34]). Webber considered that, during the spreading, the pool comes progressively in contact with surface portions being still at the temperature of the surface before the release. This means that Webber's model accounts for the different temperatures of the surface portions beneath the dynamically expanding–contracting pool. The conventional solution, available in the literature that assumes a perfect thermal contact between the pool and the underlying surface, is:

$$Q_c(t) = -\frac{\lambda A(t)\Phi(t)}{\sqrt{\pi\alpha t}} \tag{13}$$

where $\Phi(t) = T(t) - T_s$.

Webber's assumptions lead to the solution of Eq. (12) in the form:

$$Q_c(t) = -\frac{\lambda\Phi(t)}{\sqrt{\pi\alpha t}} - \frac{\lambda}{\sqrt{4\pi\alpha}}\int_0^t \frac{[\Phi(t)A(t) - \Phi(t')A(t')]}{A(t)}(t-t')^{3/2}\mathrm{d}t' \tag{14}$$

Accuracy and efficiency are crucial for the numerical evaluation of the integral in Eq. (14) at each call of the ordinary differential equations system.

Eq. (14) can be reformulated in a smarter version by introducing an approximation that does not require the numerical evaluation of the definite integral (for a detailed description see [33]):

$$Q_c(t) = \frac{k\ \Phi(t)}{\sqrt{\pi\alpha t}}\left\{-A(t) - t\ A'(t) + t^2\ \frac{A''(t)}{6}\right\} \tag{15}$$

Unfortunately, the first and second time derivatives of the pool area must be evaluated. They can be determined numerically as the backward incremental ratio or evaluated analytically from the pool radius and the first time derivatives of radial velocity.

Eq. (15) shows a singularity for $t \to 0$. To bypass the singularity, the heat conductive flux is set to zero for $t = 0$. We propose to adopt the simplified version of the vertical conduction approximation, *i.e.* Eq. (15).

3.2.5. Pool radius dynamics

According to Webber [1], the pool radius dynamics is described by the following ordinary differential equation:

$$\frac{\mathrm{d}r}{\mathrm{d}t} = u \times \phi_2(\varepsilon) \tag{16}$$

where $\phi_2(\varepsilon)$ stands for the friction term and describes the presence of a stagnant region in case of rough surfaces.

Webber did not explicitly mention how this formula should be modified when the pool reaches its minimum height and, consequently, the radial velocity is zero ($\mathrm{d}r/\mathrm{d}t = 0$). From the phenomenological point of view, when an evaporating pool reaches its minimum height, the pool starts shrinking. We propose that the radius should change according to the volume conservation. Webber's model comprises an equation to evaluate the volume dynamics, which allows making explicit the radius-time dependence:

$$r = \sqrt{\frac{V}{\pi h_{\min}}} \tag{17}$$

ABSG Consulting Inc. [17] proposed a similar approach. By using this equation, the complete pool dynamics can be simulated.

3.2.6. Turbulent mixing onto water

According to Hissong [35], a spill onto water involves a turbulent mixing between the released substance and water. This results in an increment of the heat transfer. This phenomenon can be accounted for by introducing a turbulence factor (F_T), which stands for the ratio of the actual heat transfer coefficient between water and the spreading substance (h_{act}) to the value of quiescent boiling (h_q):

$$F_T = \frac{h_{act}}{h_q} \tag{18}$$

F_T is determined experimentally by measuring the pool diameter and the evaporation rate and hence inferring the evaporative flux. From the evaporative flux and the latent heat of vaporization, the overall heat flux to the pool is then evaluated. By subtracting the radiative flux and the air convective contribute from the overall heat flux, the heat flux from water can be determined and, given the pool area and temperature, the actual heat transfer coefficient may be finally evaluated.

It was observed that during the spill onto water the turbulence factor decreases because the highly turbulent region near the spill becomes a smaller portion of the total pool area as the area increases. For LNG spills, Hissong [35] reports a heat transfer coefficient that initially is one order of magnitude higher than that evaluated assuming quiescent conditions. When the spill is over, it is three or four times higher.

According to Hissong [35], the main features influencing the turbulence factor are:

- the velocity of the released substance when it hits the water surface: at the typical release velocities the heat transfer is dominated by forced convection;
- the interfacial area between water and the spilled substance and their relative motion;
- the scale of the release.

By taking into account these key points, when modeling the turbulence factor, it is possible to improve the estimation of the heat transfer coefficient when the emission occurs. When the spillage is over, the turbulence factor becomes constant and depends only on the wind and waves. Unfortunately, there is a little knowledge about some parameters of the proposed correlation. Consequently, further experiments are needed to validate the correlation and to determine the values of the involved constants.

In Webber's model, liquids spilled onto water are assumed to float on the surface and not to mix with or to solve into it. Hissong suggests that the modeling of mixing can improve the quantification of evaporative flux for spillages onto water. Moreover, he reports that evaporation can increase three times due to mixing. This point leads some authors (*e.g.* [36]) to increase the evaporative flux, evaluated in case of pool fire onto water, by a factor of 2.5 due to the heat transfer. Probably, the mixing can explain this corrective factor.

3.2.7. Dispersion model input data

A pool can be viewed as a possible source term for a vapor cloud, meaning that the spreading model can be linked to a model for simulating the vapor cloud dispersion. By doing so, it is possible to have

a complete description of the accident evolution. The correlations we propose in this section allow describing only the buoyant or neutral gas behaviors.

The evaporating mass from the pool represents the material input data for the dispersion model. In particular, the work of Kunsch [37] describes the thickness of the concentration boundary layer (δ_c) at the pool edge (in the wind direction):

$$\delta_c = z_{0,p} \exp\left(\frac{1}{n}\right) \left[C_1 C_2 \frac{D}{z_{0,p}}\right]^{\frac{1}{1+2n}} \quad (19)$$

where:

$$C_1 = \frac{\kappa n(1+n)(1+2n)}{Sc_T \exp(1/n)} \quad ; \quad C_2 = 1 + \frac{n}{2(1+n)} \quad (20)$$

The evaporated mass passes through an imaginary rectangular area, placed at the pool edge perpendicularly to the wind direction, which has the dimensions of the pool diameter and the thickness of the concentration boundary layer. The mean mass flux ($\dot{m}_V$) can be evaluated through the mass conservation equation:

$$\dot{m}_V = \dot{m}_{ev} D \delta_c \quad (21)$$

The development of a gas dispersion module is essential for an extensive accident simulation, since there is usually a great interest in quantifying the hazardous area associated with the emission and dispersion of toxic substances. This will be a future effort of our research activity. At present, we have only laid down the input data structure of the gas dispersion module either for buoyant or for neutral gases.

3.3. Pool fire module

The aim of our research activity was not only the implementation of a dynamic simulator to describe the behavior of a liquid spilled onto a surface, but also the simulation of a pool fire produced by a pool which gets ignited during the discharge. The simulation of pool burning is relevant for determining the influence of thermal radiation on people, equipment and structures around the fire. Moreover, the influence of the fire on the process dynamics can be investigated, assuming that a certain amount of heat impinges the plant units, depending on the thermal radiation, view factors, flames and equipment areas.

Our modeling approach couples the pool spreading to fire dynamics, meaning that the evaporative flux is determined by the burning velocity, while the pool geometrical features (radius, height, ...) depend on the modified Webber's model, as explained in the previous sections. The correlations for estimating the flame geometry and emissive power are discussed in the following sections.

Generally speaking, a pool fire is defined as a buoyant diffusion flame where the fuel is arranged horizontally. According to Rew and Hulbert [38], there are two approaches to flame modeling: Computational Fluid Dynamics (CFD) models and semi-empirical models. Since the scope of our research activity is implementing a real-time simulator, the CFD approach is not practicable due to high computational times. Conversely, semi-empirical models are simpler and require reduced computational times.

Available literature models are those of Refs. [3,14,16,23,38–44].

Each model provides a methodology to evaluate the flame shape (in terms of flame length, clear flame length, drag diameter and tilt angle), the fuel burning rate, the emissive power, the atmospheric attenuation, and the view factors, because these variables determine the fire potential hazardousness. The following sections discuss the methods for their evaluation.

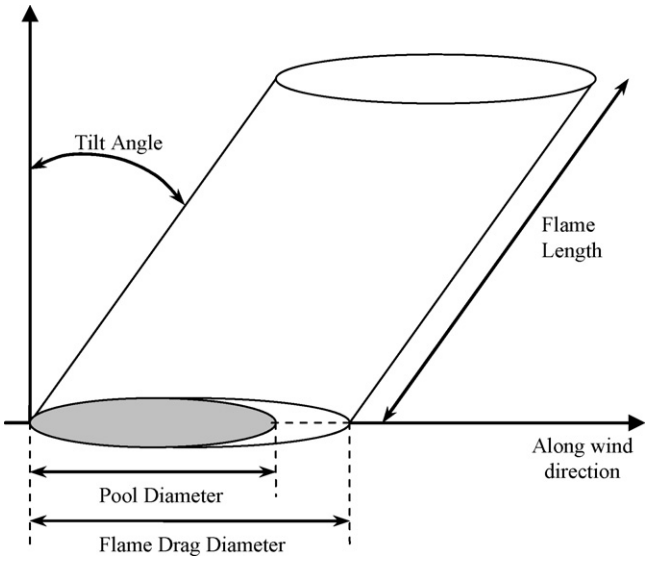

Fig. 3. Pool fire geometrical representation.

3.3.1. Flame shape

The flame shape cannot be easily and univocally described since, also under steady-state burning conditions, both its edges and top oscillate around a mean value due to the pulsating turbulent nature of the flame.

Semi-empirical models sketch the flame envelope as a cylinder or a cone, tilted along the wind direction. We chose the approach that represents the flame as a tilted elliptical cylinder characterized by a larger diameter in the wind direction, due to the wind-exerted drag (Fig. 3). Given the elliptic section of the flame, the smaller axis corresponds to the pool diameter in the cross-wind direction while the larger flame axis is equal to the drag diameter.

The top of the visible flame is defined as the section where the fuel, evaporated at the base of the pool, is completely burnt. Available correlations are reported by Rew and Hulbert [38], Society of Fire Protection Engineers [40] Society of Fire Protection Engineers [41], and Engelhard [23]. Recently, some improvements were introduced by Raj [3].

According to Raj [3], we chose to compute the flame length (L_F) as:

$$\frac{L_F}{D} = c_1 (Fr_c)^{c_2} \quad \text{for } u_F^* \le 1 \quad (22)$$

$$\frac{L_F}{D} = c_1 (Fr_c)^{c_2} (u_F^*)^{c_3} \quad \text{for } u_F^* > 1 \quad (23)$$

where the combustion Froude number (Fr_c), equivalent to a dimensionless burning rate, is:

$$Fr_c = \frac{\dot{m}_{burn}}{\rho_a \sqrt{gD}} \quad (24)$$

and the dimensionless wind speed (u_F^*) is:

$$u_F^* = \frac{u_w}{[(\dot{m}_{burn}/\rho_a) gD]^{1/3}} \quad (25)$$

The pool diameter is evaluated according to Webber's model [1]. In Eqs. (22) and (23) $c_1 = 55$, $c_3 = -0.21$ while c_2 is a discrete function of Fr_c:

- $c_2 = 2/3$ for $Fr_c \le 10^{-2}$;
- $c_2 = 0.61$ for $10^{-2} < Fr_c < 10^{-1}$;
- $c_2 = 0.4$ for $Fr_c \ge 10^{-1}$.

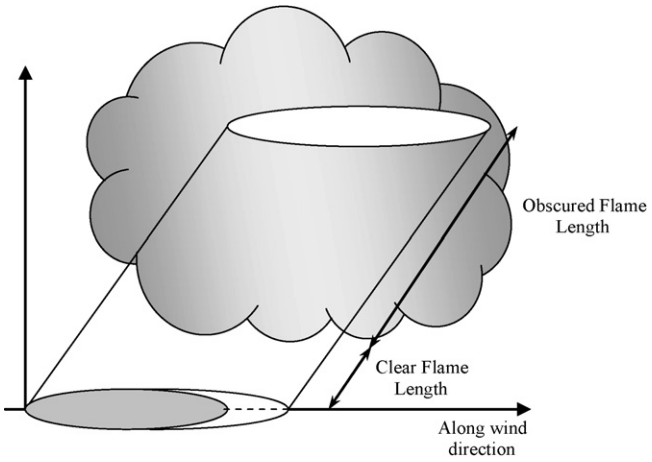

Fig. 4. Modified flame geometrical representation.

According to Engelhard [23], for pool fires onto water, no data are available for evaluating the flame length, hence the application of the same formulae developed for pool fires onto land is suggested.

As can be observed experimentally, flames are enveloped by a smoky cloud, originated by the partial combustion of fuel (see Fig. 4), meaning that the combustion products are not only carbon dioxide and water but also partially oxidized compounds (usually polycyclic aromatic hydrocarbons that form soot).

Two physical phenomena may contribute to the production of soot (generally known as smoke), even in case of "clean burning" fuels, such as LNG. The former phenomenon is the lack of enough oxygen, in the core of large-diameter fires, to burn the carbon produced by the pyrolysis of the evaporating fuel. The latter phenomenon may be explained by the decrease of the effective concentration of the evaporated fuel in the flame core due to the recirculation of burned gases by toroidal vortexes. Smoke yield, defined as the mass of smoke aerosol formed per mass of fuel consumed, depends on the burning substance. For example, Koseki and Mulholland [14] reported a comparison of smoke yield for three fuels: heptane, toluene and Arabian light crude oil. While crude oil and toluene present about the same smoke yield (0.1–0.2 g of smoke per gram of fuel burnt), heptane has a smoke yield that is an order of magnitude lower (0.05–0.015 g of smoke per gram of fuel burnt). In addition, smoke yield increases with pool diameter. Depending on the substance and the size of fire, up to 20% of the fuel mass may be converted to soot in the combustion process. This means that the smoke envelops a large portion of the flame. In particular, smoke envelopes the top of the flame.

According to Raj [16], the length of the lower part of the flame, or clear flame zone (L_C), is only a fraction of the total flame length and can be evaluated as:

$$\frac{L_C}{L_F} = 0.75 + 0.25 \cdot \log_{10}(Fr_c) \tag{26}$$

Raj [16] adapted this correlation to the experimental data measured at the Montoir LNG fire-test. Eq. (26) is valid for $Fr_c > 10^{-3}$; otherwise the clear flame length is equal to zero. In fact, such a Froude number corresponds to a LNG pool fire on water of more than 3 km of diameter. It is opinion of the Authors that the assumption of a zero clear flame length for $Fr_c > 10^{-3}$ is not so an *extreme* value.

The height of the obscured portion of the flame (L_O) at the top of the flame can be computed as:

$$\frac{L_O}{L_F} = 1 - \frac{L_C}{L_F} = 0.25[1 - \log_{10}(Fr_c)] \tag{27}$$

Another parameter describing the flame shape is the drag diameter. As aforementioned, due to the wind drag, the flame has a longer diameter in the wind direction. We chose to calculate the drag diameter (D') through Moorhouse's formula [38]:

$$\frac{D'}{D} = 1.5(Fr_{10})^{0.069} \tag{28}$$

Since Eq. (28) was validated with full-scale experimental data, such a formula is the best one in representing fires produced in real industrial accidents.

The wind has also another effect on the flame: it bends the flame in the wind direction. The tilt angle represents the deviation angle of the flame axis from the vertical. We evaluate the tilt angle through the formula proposed by Engelhard [23]:

$$\theta = \arcsin\left[\frac{\sqrt{4c^2+1}-1}{2c}\right] \tag{29}$$

where $c = 0.666(Fr_{10})^{1/3}(Re_{10})^{0.117}$.

Froude and Reynolds numbers are evaluated considering the wind velocity measured at the height of 10 m from the pool surface:

$$Fr_{10} = \frac{u_w}{gD} \tag{30}$$

$$Re_{10} = \frac{u_w D}{\nu_a} \tag{31}$$

3.3.2. Burning rate

Two models are usually cited in the literature to evaluate the burning rate ($\dot{m}_{burn}$). Both models imply empirical burning rates instead of addressing an extensive heat transfer analysis. With reference to the overall simulation framework, in case of pool fire, the evaporation rate is assumed equal to the burning rate.

Babrauskas [23] proposed the first approach. It is based on experimental data and describes the burning rate as a function of pool diameter:

$$\dot{m}_{burn} = \dot{m}_{burn,\infty}[1 - \exp(-k\beta D)] \tag{32}$$

The burning rate depends on the pool diameter because, in case of pool fire, the evaporation term is mainly due to back radiation from the flame. But, as the pool spreads, the flame reaches a diameter where it becomes optically thick, meaning that a further increase in the pool diameter does not result into a corresponding increase in back radiation. Such attenuation is accounted for by the attenuation coefficient ($k\beta$). The diameter, at which the asymptotic maximum burning rate ($m_{burn,\infty}$) is reached, depends on the burning substance. For example, for kerosene the asymptote is reached after 1.5 m while for benzene it is reached after 4.6 m. The constants and $k\beta$ can be found in the literature [23,38]. The drawback of this approach is the need of experimental data for the determination of those constants. Consequently, only the burning rate of a limited number of substances was modeled with this approach (*e.g.* methane, propane, common hydrocarbons . . .).

The second approach does not include any experimental constants. Therefore, it can be applied to any burning substances. The formula proposed by Burgess and Hertzbert [38] is:

$$\dot{m}_{burn} = c_1\left[\frac{\Delta H_C}{\Delta H^*_{ev}}\right] \tag{33}$$

For substances whose normal boiling point is higher than the ambient temperature we have $\Delta H^*_{ev} = \Delta H_{ev} + c_p(T_{eb} - T_a)$; otherwise $\Delta H^*_{ev} = \Delta H_{ev}$. In both cases $c_1 = 10^{-3}$ kg/m^{2}s.

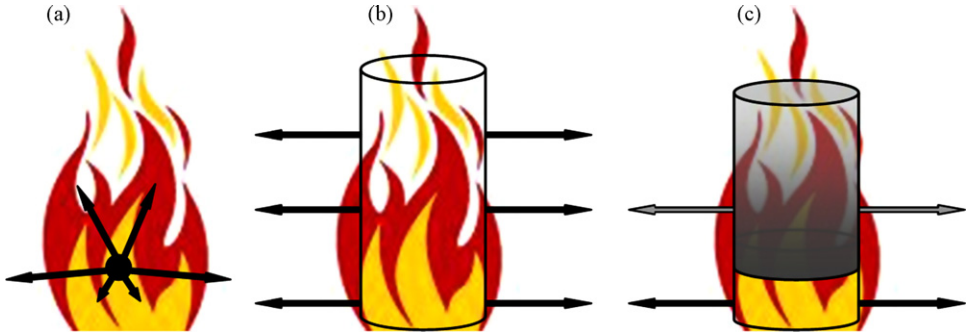

Fig. 5. Schematic representation of thermal radiation models: (a) point source model; (b) solid flame model (conventional); (c) solid flame model (modified).

An equivalent formula was proposed by Mudan and Croce [38]:

$$\dot{m}_{\text{burn}} = 1.27 \times 10^{-6} \rho_{\text{L}} \frac{\Delta H_{\text{C}}}{\Delta H^{*}_{\text{ev}}} \tag{34}$$

where 1.25×10^{-6} is measured in m/s.

Babrauskas [23] derived a correlation accounting for the wind speed in the form:

$$\frac{\dot{m}_{\text{burn,wind}}}{\dot{m}_{\text{burn}}} = 1 + 0.15 \frac{u_{\text{w}}}{D} \tag{35}$$

where the constant 0.15 is measured in s. This formula is valid neither for alcohols nor for fire blown-outs (approximately at wind speeds over 5 m/s). The wind influence is relevant, it can even double the burning rate.

We decided to adopt Eq. (32) when experimental data are available; otherwise Eq. (34) is preferred because it shows a better agreement with experimental data than Eq. (33) [38]. The correction accounting for the wind speed was also included in our model.

Both the approaches of Babrauskas (Eq. (32)) and Mudan and Croce (Eq. (34)) can be applied only to spills onto land [35,38]. For pool fires onto water there are no formulae available in the literature. It was observed that the burning rates of crude oil and gasoline onto either land or water do not show a significant difference, while for LPG, liquefied petroleum gas, the burning rate onto water is about twice higher than that onto land, and for LNG about three times. Consequently, different values of $\dot{m}_{\text{burn},\infty}$ and $k\beta$ are reported in the literature for fires onto land or water. We chose to apply Eqs. (32) and (34) both to fires onto land and onto water.

3.3.3. Surface emissive power

The most important parameter in modeling pool fires is the emissive power of the flame that is required to evaluate the radiated heat flux impinging the surrounding surfaces.

As happens for the burning rate, some empirical correlations model the surface emissive power (SEP). The first difference among the correlations reported in the literature lies in the representation of the radiant source. Two approaches were developed: the point source model (Fig. 5a) and the surface emitter model (Fig. 5b and c).

The point source model is accurate in the far-field, *i.e.* beyond five pool diameters from the center of the flame [23]. Conversely, it is overly conservative within a distance of a few fire diameters because it assumes that all the radiative energy is emitted from a single point rather than being distributed over an idealized surface, usually a cone or cylinder, representing the fire envelope.

The conventional solid flame radiation model describes the fire as a vertical cylinder emitting a thermal radiation from its surface. We chose to implement the modified solid flame model, to account for the flame obscuration due to soot. Modeling the surface emissive power, to account for the differences between the bottom and top portions of the flame, is recommended and also supported by experimental data from on land LNG pool fires of 35 m diameter (carried out in Montoir, France in 1987), such as those showing a surface emissive power variability of a factor of five [44]. Moreover, this choice is supported by the National Institute of Standards and Technology (NIST) guidelines for thermal radiation [42]. These guidelines report that, for certain fire scenarios, the conventional solid flame model may produce estimates of the radiative flux that are up to an order of magnitude larger than those really measured in in-field experiments. These results are obtained by a wrong use of the conventional model that assumes that the smoke does not obscure large fires.

With the modified solid flame radiation model, the overall surface emissive power is evaluated by assuming that it is the sum of both the emissive powers of the clear flame zone and the obscured zone, uniformly distributed over the whole flame surface. According to this approach, Engelhard [23] and Pula et al. [43] modeled the flame surface emissive power (E) as:

$$E = xE_{\text{C}} + (1 - x)E_{\text{Soot}} \tag{36}$$

where x is the unobscured length ratio ($L_{\text{C}}/L_{\text{F}}$). Usually, the unobscured ratio is assumed to be one-fifth of the total flame height, if the clear flame length is unknown. The surface emissive power of the obscured zone (E_{Soot}) is usually assumed to be 20 kW/m^2. The surface emissive power of the clear flame portion (E_{C}) can be evaluated through the Babrauskas [23] approach:

$$E_{\text{C}} = E_{\infty}[1 - \exp(-k_{\text{burn}} D)] \tag{37}$$

where E_{∞} is the maximum surface emissive power of a substance and k_{burn} is the extinction coefficient. Alternatively, the surface emissive power can be evaluated as [23]:

$$E_{\text{C}} = F_{\text{S}} \frac{\dot{m}_{\text{burn}}\ \Delta H_{\text{c}}}{1 + 4\left(L_{\text{C}}/C\right)} \tag{38}$$

Both the approaches require some empirical constants: E_{∞} and k_{m} in Eq. (37) and F_{S} in Eq. (38). Consequently, only the surface emissive power of a limited number of substances can be modeled by these approaches. For all the other cases the alternative is Ref. [23]:

$$E = 140 \times 10^{3} \exp(-0.12D) + 20 \times 10^{3}[1 - \exp(-0.12D)] \tag{39}$$

In this correlation, a constant value for the emissive power of the unobscured flame portion is assumed, whose suggested value is 140 kW/m^2. In addition, a constant similar to an extinction coefficient is introduced with a value of 0.12. This value is based on the experimental evidence that the surface emissive power decreases when increasing the diameter, till reaching an asymptote for diameters larger than approximately 30 m.

We chose to adopt Eq. (37) for evaluating the surface emissive power of the clear flame portion and Eq. (36) for the total surface emissive power, if tabular data are present in the literature. Otherwise, Eq. (39) is preferred.

By applying Eq. (36), it is possible to appreciate the difference between the surface emissive power estimates produced by the conventional and the modified solid flame radiation model. Let us consider a toluene pool fire, whose maximum surface emissive power is 130 kW/m^2 [38]. The surface emissive power in case of unobscured flames is clearly 130 kW/m^2. Assuming that the unobscured ratio is one-fifth of the total flame height, the surface emissive power becomes 42 kW/m^2. The surface emissive power is then reduced by more than 70%, meaning that the modeling of smoke obscuration is highly recommended to obtain physically sound results.

3.3.4. Entrained mass of air

The mass of air entrained into the flame determines the flame size and shape, the degree of mixing and hence the smoke production, the radiative emission, and the fuel consumption. Entrainment rate is defined [39] as the change in the axial mass flow rate of air along the flame vertical axis:

$$\dot{m}_a = 2\pi \frac{d}{dz} \int_0^{D/2} \rho v r dr \tag{40}$$

According to Raj [16], the entrained mass of air ($\dot{m}_a$) can be evaluated under the following hypotheses:

- the entrainment of air occurs at the periphery of the fire envelope;
- the air entrainment rate at height z is proportional to the local upward velocity of gases measured at that height. The local upward velocity is the velocity of gases averaged over the horizontal section of fire at a given height;
- the mean upward velocity of gases at a given height is proportional to the square root of z;
- only a fraction of the entrained oxygen burns.

Last point is accounted for by introducing a variable, η, representing the mass fraction of entrained air that stoichiometrically reacts with the fuel. The inverse of η is the ratio between the mass of entrained air and the stoichiometric mass necessary for complete combustion. Therefore, the entrained mass of air can be evaluated as:

$$\dot{m}_a = \frac{r_{st}}{\eta} \dot{m}_{burn} \tag{41}$$

where r_{st} is the stoichiometric air to fuel mass ratio. The value of η can be evaluated by numerically solving the following equation:

$$\frac{r_{st}}{\eta}\left[\left(\frac{9}{128\alpha_e Da}\right)\left(1+(Da)\frac{\eta}{r_{st}}\right)\right]^{1/3} = 55 \tag{42}$$

where Da is the Damkholer number:

$$Da = \frac{\Delta H_C}{(c_{p,a} T_a)} \tag{43}$$

The value of η depends only on the substance, being independent from the flame dimensions. By solving Eq. (42), the value of η is determined, and consequently the total air entrained in the flame. This allows evaluating the mass forming the flame and afterwards the mass of the cloud of combustion products, entrained air and smoke. These data can be the input for modeling the gas dispersion, as discussed in Section 3.2.7.

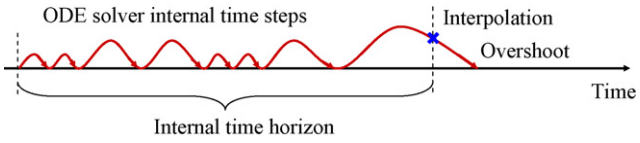

Fig. 6. ODE solver jumps within an internal time horizon.

3.3.5. Concluding remarks on the pool fire module

In previous sections, the authors suggested a number of modifications to improve Webber's model [1] for modeling pool spreading and evaporation. The authors discussed also the selection of correlations for modeling pool fires.

In order to validate the model for pool spreading, evaporation and burning, a comparison with experimental data is mandatory. The following section presents the validation of the model, where the effectiveness of the model in reproducing experimental data is outlined.

4. Simulation framework

Previous sections pointed out the strengths and drawbacks of several models and correlations, discussed in the literature, for the development of a consistent model. This section discusses how these correlations should be combined together to produce a unified model.

The model that describes the pool dynamics requires the solution of either six (spreading phase) or four (shrinking phase) ordinary differential equations. To speed up the simulation, we adopted VODE a variable coefficients, multivalue, and variable time step ODE routine [45] capable of integrating both stiff and non-stiff problems. Given a simulation time horizon, this solver modifies automatically the time step to integrate the ODE system according to the stiffness of the problem [46]. Therefore, to evaluate the variables at the output time chosen by the user, the solver goes through a number of intermediate steps that depend on the problem. Since some input variables may vary in time (*e.g.* the discharge rate, the wind speed, the cloud cover), the ODE solver is forced to simulate time horizons (*i.e.* internal time horizons, see also Fig. 6) that are smaller than the total time horizon.

Common values of the internal time horizon are 0.25–0.5 s, while the total time horizon may be tens of minutes. This means that:

- the total time horizon is subdivided into smaller sampling times that reflect the variability of some inputs;
- within each internal time horizon, the solver goes through a suitable number of steps, depending on the stiffness of the system. The user does not receive any feedbacks about the internal time steps performed by the solver.

To determine the value of the variables at the end of each internal time horizon, the simulator:

(1) checks the consistency of the inputs that are modified;
(2) initializes the dependent variables of the differential system;
(3) solves the ODE system over the internal time horizon.

With reference to point (3), the simulator:

(3a) evaluates the physicochemical properties of the pool at the instantaneous pool temperature;
(3b) evaluates each term of the differential equations.

Every time a successful step is done:

(1) the solver checks whether the pool height is over its minimum value. If not, the solver forces the pool height to the minimum value, and reevaluates the pool radius accordingly;
(2) the solver checks that the pool temperature does not exceed the boiling point. If this happens, it is due to the numerical tolerance of the ODE solver and not to a wrong energy balance. Consequently, the solver forces the pool temperature to be equal to the boiling point;
(3) if a bund is present, the solver checks that the pool radius does not exceed the bund radius. This is another example of numerical precision/tolerance. If so, the solver forces the pool radius to be equal to the bund radius and reevaluates the pool height accordingly.
(4) the solver checks if there is a change in the pool regime, *i.e.* the pool starts shrinking while at the previous time step it was spreading and *vice versa*. If so, the simulation is reinitialized with a switch between the ODE systems governing these physical phenomena.

If the pool is not ignited and if the pool temperature is lower than the boiling point, we adopt Eq. (5) to evaluate the evaporation rate. If the pool is boiling, the evaporation rate comes from the energy balance.

If the pool is ignited, the evaporation rate is evaluated in terms of burning rate, *i.e.* by Eqs. (36) or (39), and the ODE solver evaluates also the flame properties, as discussed in Section 3.3.

5. Model validation

Once the theoretical framework for describing the physical phenomenon of pool spreading, evaporation and burning has been developed, the comparison of simulated and experimental data allows determining the correctness of the proposed hypotheses, assumptions and simplifications. Consequently, the following step of our work consists in comparing different sets of experimental data with the model outputs. This comparison was not trivial since experimental reports are often not easy to find and the input data necessary to perform a simulation of the in-field tests are not extensively and exhaustively reported. Hence, due to the limited number of exhaustive literature sources, we chose to simulate the spreading of water in a bund [2] and the LNG spills onto water with prompt ignition [3]. The following sections discuss these comparisons.

5.1. Spreading of water in a bund

In order to validate the model portion related to spreading, we compared the experimental data of Cronin and Evans [2] with simulated data.

Cronin and Evans [2] carried out a series of experiments to study the spreading of water pools with different bund arrangements (circular and square bunds). The vessel, from which the water was released, was designed to represent a quadrant of a 70 m diameter storage tank on a 1/20th scale. Hence, the radius of the tank used in the experiments was 3.5 m. The tank was filled with different amounts of water at ambient temperature, ranging from 3.5 to 4.3 m^3. The liquid release mechanism was put at the bottom of the tank, approximately at 2 cm from the ground, allowing the water to flow from the tank onto a concrete pad. The movement of water across the bund floor was monitored by 60 resistance probes, fixed on the concrete bund floor. The resistance probes were set at different distances and different angles from the tank center. The wetting times were measured with an accuracy of less than 1 ms [2].

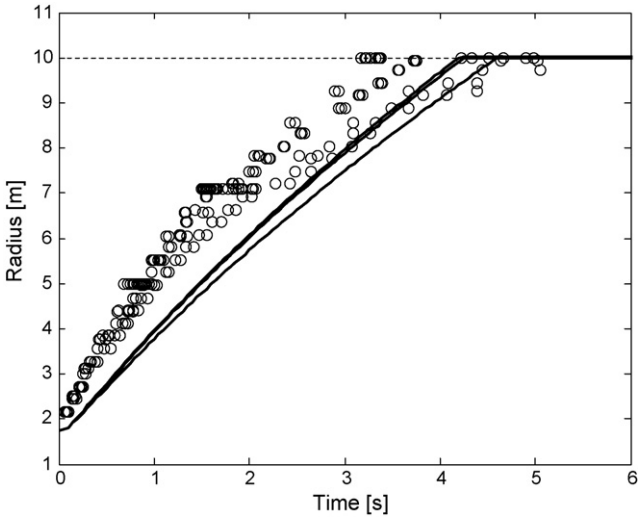

Fig. 7. Comparison of experimental results (circle) and simulated data (solid line) for water spreading within a 10 m bund.

Cronin and Evans' experiments involved three circular bunds with diameters of 5, 7.1, and 10 m. In the first two cases, the spreading lasted less than 2 s, where our model is not valid for spreading times lower than 1 s [47]. Therefore, we validated our model only with the third set of data, which is related to water spreading into a 10 m bund. Five experiments were carried out, by varying the initial water height in the tank (1.449, 1.880, 1.808, 1.800, and 1.805 m).

Fig. 7 shows the comparison of experimental and simulated data. The pool radius is measured from the tank center. Therefore, a radius equal to 1.75 m corresponds to the tank edge, where the release occurs.

Simulated results are in quite good agreement with experimental data, especially in terms of time at which the water reaches the bund. We want to remark again that, before 1 s, the differences between the model and the experimental data are intrinsic to the model limits. According to this specific validation, we can state that the spreading model is good enough in reproducing experimental data.

5.2. LNG spills onto water

The second data-set is a series of six tests performed by spilling from 3 to 5.5 m^3 of LNG onto water, with spill rates of 0.02–0.11 m^3/s at the Naval Weapons Center at China Lake, California [48]. This allows validating two coupled phenomena: pool spreading and pool burning.

The experiments involving the immediate ignition of LNG pools are reported by Raj [3]. Unfortunately, Raj did not report the environmental conditions in detail. Hence, we assumed that the tests were carried out at 2 p.m. in June, with the wind speeds reported by Rew and Hulbert [38], clear sky, ambient temperature of 30 °C and

Table 5
Experimental conditions [38,3]

Experiment no.	Spilled volume (m^3)	Flow rate (m^3/s)	Release time (s)	Wind speed (m/s)
1	5.3	2.09E-2	254	0.0
3	4.2	8.57E-2	49	0.0
4	4.2	1.69E-2	248	2.2
5	3.0	9.38E-2	32	0.9
6	5.7	10.96E-2	52	2.6
8	5.7	7.04E-2	81	0.0

Table 6
Comparison between experimental [3] and simulated values

Experiment no.	Experimental flame diameter	Simulated flame diameter (m)	Experimental flame length (m)	Simulated flame length (m)	Experimental SEP (kW/m^2)	Simulated SEP (kW/m^2)
1	8.5	8.8	24.0 ± 2.7	31.6	–	184
3	11.5	12.1	47.2 ± 3.9	44.6	207 ± 5	214
4	9.0	9.0	25.5 ± 6.3	28.8	200 ± 11	187
5	12.8	10.4	55.0 ± 8.5	38.3	187 ± 29	200
6	15.0	15.2	42.0 ± 6.4	49.4	185 ± 6	231
8	14.0	13.8	44.0 ± 6.3	51.5	224 ± 13	224

30% of relative humidity. The latitude of the test field was assumed to be 35°N.

Table 5 summarizes the release conditions, while Table 6 shows a comparison between experimental data and simulation results. In Table 6, the experimental flame diameter for test number 6 is the mean value between the values in the along-wind and cross-wind direction values.

In this particular series of tests, the flames were not obscured by any smoke (see the photo in Raj's paper at page 451, [3]). Therefore, the data reported in the last column of Table 6 are evaluated by Eq. (37), assuming that no smoke is present. As can be seen in the photos of other experimental tests, usually large pool fires develop a large amount of smoke. So, we suggest using Eq. (36) for all the other cases.

The simulated values of flame diameter and flame length are in good agreement with the experimental data. The surface emissive powers are usually overestimated, the larger error being ∼20% higher than the experimental value.

It is possible to conclude that simulation results are representative of the phenomenon, even for the surface emissive power. In fact, to account for model uncertainties, a "safety factor" is introduced in the evaluation of the exposed areas with respect to the acceptable thresholds, where Guidelines and Directives define the thresholds. The safety factor recommended in estimating the surface emissive power is usually: two [40,41]. From this point of view, the results of our model, concerning the surface emissive power, are within the model uncertainties.

These comparisons did not allow validating the evaporation model, but a discussion about the accuracy of such a model can be found in the work of Brighton [12].

6. Conclusions

This manuscript focused on the development of a unified model for the simulation of pool spreading, evaporation and burning. To make feasible the coupling of an accident simulator to a process dynamic simulator, we were forced to select some simplified, and not demanding models in terms of computational effort.

Webber's model [1] was assumed as the basis for modeling pool spreading and evaporation. With respect to other simplified models reported in the literature (*e.g.* [5,19]), Webber's model was preferred because of:

- it is suited for modeling both evaporating and non-evaporating substances;
- it includes the friction term in the equation for describing the pool spreading dynamics;
- the evaporation model does not imply any experimental and dimensional constants;
- it does not include any algebraic equations;
- it models more rigorously the conductive heat flux between the pool and the ground.

We presented, discussed and included in our unified model some improvements, derived from several literature studies. In particular, the improvements regarded: friction term in presence of film boiling [17,29]; friction velocity [4,30]; wind profile index [32]; conductive heat flux [33]; radius-time dependence at the pool minimum thickness [17]; turbulent mixing onto water [35]; dispersion model input data for buoyant and neutral gases [37].

To validate our unified model, we carried out some comparisons with literature data. In particular, we showed that the unified model is good in reproducing experimental data. The comparison with Cronin and Evans [2] data, on a continuous, time-varying water release, showed that the portion of the model related to spreading is effective in reproducing experimental data (see Section 5.1). On the other hand, the capability of coupling pool spreading to pool burning was proven by the comparison with experimental data reported by Rew and Hulbert [38] and Raj [3] (see "Abstract" section). Simulated pool radius, flame height and surface emissive power were compared with the experimental data, demonstrating a good agreement.

Therefore, it is possible to conclude that the unified model is representative of the real phenomena. It can be implemented whenever prompt responses are mandatory, *e.g.* in case of a chemical accidents, to assist first responders with easily accessible and accurate information about the possible accident dynamics, as well as for training purposes of both control room and in-field operators.

From this point of view, an advisable future development of our research activity is the "real-time" modeling of gas dispersion in complex environments, such as chemical facilities and urban areas.

References

[1] D.M. Webber, A Model for Pool Spreading and Vaporization and its Implementation in the Computer Code G*A*S*P, AEA Technology, SRD/HSE/R507, 1990.
[2] P.S. Cronin, J.A. Evans, A series of experiments to study the spreading of liquid pools with different bund arrangements, Advantica Technologies Limited, HSE Contract Research Report 405/2002, 2002.
[3] P.K. Raj, LNG Fires: a review of experimental results, models and hazard prediction challenges, J. Hazard. Mater. 140 (2007) 444–464.
[4] O.G. Sutton, Micrometeorology, McGraw Hill, New York, 1953.
[5] J.A. Fay, The spread of oil slick on calm sea, in: D.P. Hoult (Ed.), Oil on the Sea, Plenum Press, Cambridge, MA, 1969.
[6] C.J.H. van der Bosch, Interfacing of models, in: Methods for the Calculation of Physical Effects due to Releases of Hazardous Materials (Liquids and Gases), C.J.H. van der Bosch, R.A.M.P. Weterings (Eds.), Gevaarlijke Stoffen, Netherlands, 2005.
[7] D.P. Hoult, Oil spreading on the sea, Annu. Rev. Fluid Mech. 4 (1972) 341–368.
[8] H.R. Chang, R.C. Reid, J.A. Fay, Boiling and spreading of liquid nitrogen and liquid methane on water, Int. Commun. Heat Mass Transfer 10 (1983) 253–263.
[9] D.M. Webber, P.W.M. Brighton, Inviscid similarity solutions for slumping from a cylindrical tank, Trans. ASME 108 (1986) 238–240.
[10] M. Apel-Paz, A. Marmur, Spreading of liquids on rough surfaces, Colloids Surf., A: Physicochem. Eng. Aspects 146 (1999) 273–279.
[11] D. MacKay, R.S. Mastugu, Evaporation rates of liquid hydrocarbons spills on land and water, Can. J. Chem. Eng. 31 (1973) 434–439.
[12] P.W.M. Brighton, Evaporation from a plane liquid surface into a turbulent boundary layer, J. Fluid Mech. 159 (1985) 323–345.
[13] B.J. McCaffrey, Purely Buoyant Diffusion Flames: Some Experimental Results, Center of Fire Research, NBSIR 79-1910, 1979.

[14] H. Koseki, G.W. Mulholland, The effect of diameter on the burning rate of crude oil pool fires, Fire Technol. 27 (1991) 54–65.
[15] J.A. Fay, Spread of large LNG pools on the sea, J. Hazard. Mater. 140 (2007) 541–551.
[16] P.K. Raj, Large hydrocarbon fuel pool fires: physical characteristics and thermal emission variation with height, J. Hazard. Mater. 140 (2007) 280–292.
[17] ABSG Consulting Inc., Consequence Assessment Methods for Incidents Involving Releases from Liquefied Natural Gas Carriers, for the FERC (Federal Energy Regulatory Commission) under contract number FERC04C40196, 2004.
[18] T.K. Fannelop, Fluid Mechanics for Industrial Safety and Environmental Protection, Elsevier Science Ltd., Amsterdam (Netherland), 1994.
[19] H.W.M. Witlox, Model for pool Spreading, Evaporation and Solution on Land and Water (PVAP) – Theory Manual, Consequence modeling documentation (PHAST Technical Reference), 2000.
[20] D.M. Webber, Source terms, J. Loss Prev. Process Ind. 4 (1991) 5–15.
[21] D.M. Webber, Model for Pool Spreading, Evaporation and Solution on Land and Water (PVAP) – Verification Manual, in PHAST 6.0 Manual, 2000.
[22] C. Conrado, V. Vesovic, The influence of chemical composition on vaporisation of LNG and LPG on unconfined water surfaces, Chem. Eng. Sci. 55 (2000) 4549–4562.
[23] W.F.J.M. Engelhard, Heat flux from fires, in: Methods for the Calculation of Physical Effects due to Releases of Hazardous Materials (Liquids and Gases), C.J.H. van der Bosch , R.A.M.P. Weterings (Eds.), Gevaarlijke Stoffen, Netherlands, 2005.
[24] J.A. Fay, Private communication, 2007.
[25] C.H. Huang, Pasquill's influence: on the evaporation from various liquids into the atmosphere, J. Appl. Meteorol. 36 (1997) 1021–1026.
[26] R.H. Perry, D.W. Green, Perry's Chemical Engineers' Handbook, seventh ed., Mc Graw-Hill, New York, 1997.
[27] C.J.H. van der Bosch, Pool evaporation, in: Methods for the Calculation of Physical Effects due to Releases of Hazardous Materials (Liquids And Gases), van der C.J.H. Bosch , R.A.M.P. Weterings (Eds.), Gevaarlijke Stoffen, Netherlands, 2005.
[28] P.W.M. Brighton, Private communication, 2006.
[29] FERC Commission, Notice of Availability of Staff's Responses to Comments on the Consequence Assessment Methods for Incidents Involving Releases from Liquefied Natural Gas Carriers, Docket No. AD04-6-000, 2004.
[30] A.P. van Ulden, A.A.M. Holstlag, Estimation of atmospheric boundary layer parameters for diffusion applications, J. Climate Appl. Meteorol. 24 (1985) 1196–1207.
[31] H.C. Goldwire, H.C. Rodean, R.T. Cederwall, E.J. Kansa, R.P. Koopkman, J.W. McClure, T.G. Rae, L.K. Morris, L. Kamppinen, R.D. Kiefer, P.A. Urtiew, C.D. Lind, Coyote Series Data Report LLNL/NWC 1981 LNG Spill Tests Dispersion, Vapor Burn, and Rapid Phase Transition, UCID – 19953, vol. 1, 1983.
[32] F.P. Lees, Loss Prevention in the Process Industries, Third ed., Elsevier, Oxford, 2004.
[33] D.M. Webber, Heat Conduction Under a Spreading Pool, SRD R421, 1987.
[34] F.P. Incropera, D.P. De Witt, Fundamentals of Heat and Mass Transfer, sixth ed., John Wiley & Sons, New York, 2006.
[35] D.W. Hissong, Keys to modeling LNG spills on water, J. Hazard. Mater. 140 (2007) 465–477.
[36] DNV, Theory manual, Version 6.5, 2007.
[37] J.P. Kunsch, Two-layer integral model for calculating the evaporation rate from a liquid surface, J. Hazard. Mater. 59 (1998) 167–187.
[38] P.J. Rew, W.G. Hulbert, Development of a Pool Fire Thermal Radiation Model, HSE Contract Research Report no. 96/1996.
[39] X.C. Zhou, J.P. Gore, Measurements and prediction of air entrainment rates of pool fires, in: Combustion Institute, Symposium (International) on Combustion, 26th Proceedings, vol. 1, Napoli, Italy, Combustion Institute, Pittsburgh, PA, 1996, pp. 1453–1459.
[40] Society of Fire Protection Engineers, Assessing Flame Radiation to External Targets from Pool Fires, Engineering Guide, m06/26355, 1999.
[41] Society of Fire Protection Engineers, Engineering Guide: Assessing Flame Radiation to External Targets from Pool Fires, Society of Fire Protection Engineers Society of Fire Protection Engineers, 1999.
[42] K.B. McGrattan, H.R. Baum, A. Hamins, Thermal Radiation from Large Pool Fires, Fire Safety Engineering Division Building and Fire Research Laboratory, NISTIR 6546, 2000.
[43] R. Pula, F.I. Khan, B. Veitch, P.R. Amyotte, Revised fire consequence models for offshore quantitative risk assessment, J. Loss Prev. Process Ind. 18 (2005) 443–454.
[44] P.K. Raj, Spectrum of Fires in an LNG Facility. Assessments, Models and Consideration in Risk Evaluations – Final Technical Report, submitted to the U.S. Department of Transportation Pipeline & Hazardous Materials Safety Administration, Contract Number: DTRS56-04-T-0005, 2006.
[45] P.N. Brown, G.D. Byrne, A.C. Hindmarsh, VODE: a variable coefficient ODE solver, SIAM J. Sci. Stat. Comput. 10 (1989) 1038–1051.
[46] L.F. Shampine, in: R.C. Aiken (Ed.), What is Stiffness? Stiff Computation, Oxford University Press, New York, 1985.
[47] D.M. Webber, S.J. Jones, A model of spreading vaporising pools, in: Woodward (Ed.), International Conference on vapor Cloud Modelling, AIChE, Boston, Massachusetts, USA, 1987.
[48] M. Hightower, L. Gritzo, A. Luketa-Hanlin, J. Covan, S. Tieszen, G. Wellman, M. Irwin, M. Kaneshige, B. Melof, C. Morrow, Guidance on Risk Analysis and Safety Implications of a Large Liquefied Natural Gas (LNG) Spill Over Water, Sandia National Laboratories, SAND2004-6258, 2004.